ZnTe/Zn(S,Te) superlattices: A relaxation study by x-ray diffraction and reflectometry

M. Korn, M. Li, S. Tiong-Palisoc, M. Rauch, and W. Faschinger
Physikalisches Institut, EP III, Am Hubland, 97074 Würzburg, Germany
(Received 3 August 1998)

Two different x-ray techniques, high resolution x-ray diffraction and reflectometry, are applied to investigate crystallinity and interface properties of $ZnS_{0.8}Te_{0.2}$/ZnTe strain-balanced superlattices as a function of their period. To gain a conclusive picture, the reciprocal space is probed in different regions: Measurements around the (004) Bragg peak allow conclusions on island formation and relaxation: For a superlattice period below 2 nm the layers and interfaces are nearly perfect. At periods above 2 nm there is a spread in the average lattice constant, indicating the formation of ZnTe islands. Finally, at periods above 2.4 nm the critical thickness of the ZnTe layers is exceeded, and dislocations are observed as a spread in the lattice plane orientation. Reflectometry scans, that probe a region close to the origin of reciprocal space, give complementary information and help to quantify the interface roughness: The nearly perfect sample with the lowest period exhibits a pronounced structure of very regular terraces with bunched steps, so that the interfaces are strongly anisotropic. The roughness in the vertical direction is very low, and is inherited from layer to layer. With increasing period, one observes an increase of the vertical roughness due to island formation and a decrease of the anisotropy due to step wandering. Direct imaging methods like atomic force microscopy and transmission electron microscopy essentially confirm these results, but do not give much additional information. [S0163-1829(99)15415-8]

INTRODUCTION

Optoelectronic devices in the near-infrared and red spectral range are typically based on GaAs and $Al_xGa_{1-x}As$, with GaAs used as an easily available high-quality substrate material. On the other end of the visible spectrum, the II–VI semiconductor ZnSe has the same crystal structure and nearly the same lattice constant, a fact that has led to the development of high-quality light emitters[1] and detectors[2] in the blue range of the spectrum that are also based on GaAs as a substrate. The availability of additional materials lattice matched to GaAs with energy gaps corresponding to the wavelengths between red and blue would thus allow on to cover the entire visible range with devices based on the same substrate. One of the best candidates that fulfills these requirements is the alloy ZnS_xTe_{1-x}, which can be lattice matched to GaAs for a Te content of about 35%, and then exhibits an energy gap of about 2.2 eV. The corresponding combination of ZnS and ZnTe to a superlattice lattice matched to GaAs would be still more flexible, since for a superlattice the energy gap at a given lattice constant can be changed by a variation of the superlattice period. Unfortunately, the optimum substrate temperatures for molecular-beam-epitaxy (MBE) growth of ZnS and ZnTe differ considerably, so that high-quality ZnS/ZnTe superlattices cannot be grown by MBE. This problem can be solved by the use of ZnS_xTe_{1-x} with a low Te content (typically 20%) instead of ZnS as one component of the superlattice, since a common substrate temperature of 280 °C is suited for both ZnTe and $ZnS_{0.8}Te_{0.2}$ growth.[3] $ZnS_{0.8}Te_{0.2}$/ZnTe superlattices are thus of considerable interest for optical devices, and efficient pin detectors with external quantum efficiencies up to 60% have recently been fabricated in our laboratory from such superlattices lattice matched to GaAs.[4]

In addition to this device aspect, such superlattices are of interest from a more fundamental point of view: They are formed from individual layers with a very large lattice mismatch with respect to the GaAs (8% for ZnTe, and 2% for $ZnS_{0.8}Te_{0.2}$) that must be exactly strain balanced in order to obtain high-quality material. Due to this high built-in strain, this system offers an interesting model system for which effects like interface roughening and relaxation of the individual layers can be studied. We have recently shown that such superlattices can be grown in excellent quality.[4] In this paper we use x-ray-diffraction techniques to obtain a detailed understanding of the evolution of interface properties and crystalline quality with increasing superlattice period, and compare the obtained results to direct imaging techniques like atomic force microscopy (AFM) and transmission electron microscopy.

EXPERIMENTAL DETAILS

ZnTe-Zn(S,Te) superlattices were grown on (001)-GaAs substrates. A series of lattice-matched samples with different superlattice periods was grown in the following way: first a 400-nm GaAs buffer layer was grown on the substrate. The sample was then transferred under ultrahigh vacuum to a II–VI growth chamber. Here a 20-nm ZnSe buffer layer was deposited, followed by the ZnTe-ZnS_xTe_{1-x} superlattice structure grown at a substrate temperature of 280 °C. For the superlattice, a group-II rich flux ratio was used. Zinc and tellurium were evaporated from elemental cells, while sulfur was evaporated from a ZnS compound source. After the deposition of each individual layer, growth was interrupted and the surface was exposed to a molecular beam of zinc for 10 sec to smooth the surface.

For all samples, the number of superlattice periods was chosen to be 20, making it possible to obtain ω-2θ-reflectometry scans with finite thickness fringes resolved. A sulfur content of 20% for the ZnS_xTe_{1-x} barrier was chosen. For a lattice-matched sample the ratio between the ZnTe well

TABLE I. Results obtained from HRXRD.

Sample No.	Period (Å)	Lattice mismatch (%)	Superlattice thickness (nm)	γ (%)	$FWHM_{mea\ z}$ (arcsec)	$FWHM_{sim\ z}$ (arcsec)	$\Delta FWHM_z$ (arcsec)	$\Delta FWHM_x$ (arcsec)
1	19.2	0.63	39.2	1	410	407	3	0
2	23.9	0.86	47.8	1	387	355	32	1
3	32.8	0.19	65.6	1	276	196	80	17
4	40.9	≈0	81.8		550	202	348	26

thickness and the $ZnS_{0.8}Te_{0.2}$ barrier width is approximately 1:2. The series consisted of four lattice-matched samples with intended periods of 20, 24, 32, and 40 Å (the corresponding sample numbers are 1, 2, 3, and 4). The sample structures are listed in Table I.

The main focus of our investigation is on x-ray-diffraction techniques. As shown in our first study devoted to ZnS, Te-related superlattices,[5] high-resolution x-ray-diffraction (HRXRD) around Bragg peaks is a very powerful tool to determine the onset of the relaxation process such as island or dislocation formation. With HRXRD it is possible to distinguish between a variation in the lattice constant, as it occurs in the case of elastic island formation, and a variation of the lattice plane orientation, which is a measure for misfit dislocation formation, by measuring the full width of half maximum (FWHM) of the Bragg peaks in directions parallel and vertical to the surface, respectively (hereafter called q_x and q_z direction). For HRXRD measurements the following x-ray optics was used: on the incident side an x-ray mirror together with a four-crystal Ge 220 monochromator; and on the exit side a 1° receiving slit (for q_z scans) or a triple-axis Ge 220 monochromator (for q_x scans).

Second, grazing-incidence x-ray scattering measurements were carried out, using the same diffractometer equipped with an x-ray mirror and a programmable divergence slit. With these experiments one probes the reciprocal space close to the origin, so that one is especially sensitive to interface properties. Specular and nonspecular scattering of x rays contains statistical information about the interfacial structure which can be accessed by employing a model based on the distorted-wave Born approximation to evaluate the reflectivity data.[6] This is an excellent tool for the investigation of the mesoscopic structure of heterostructures, such as the interface roughness and the correlation between different interfaces.

To obtain a comprehensive picture, these x-ray methods were complemented by AFM and TEM. While x-ray methods give statistical informations over large sample areas, these direct imaging techniques are complementary in the sense that they probe very small sample areas with high spacial resolution.

RESULTS AND DISCUSSION

In order to determine the relaxation degree γ, asymmetric 113 and 115 reflections were also measured. The resulting values for γ are included in Table I. Sample Nos. 1–3 have a γ of 1, corresponding to a fully strained situation with respect to the substrate. For sample No. 4 the asymmetric reflexes were too weak to be measured. This indicates a strong peak broadening, so that this sample is presumably partly relaxed.

Second, symmetric reflexes were investigated. Figure 1 shows ω-2θ scans of sample Nos. 1–4, measured around the symmetric 004 reflection of the GaAs substrate. Such scans give information on variations of the lattice constant in the growth direction and on interference phenomena occurring in this direction. To describe the typical features of such a scan, we concentrate first on the results for sample No. 2: Superlattice satellite peaks can be observed in an ω range of 10°. On the left side of the ω-2θ curve, superlattice satellites up to the third order are visible, while on the right side only the the first-order superlattice peak is observed. Between the satellites of -1 and $+1$ order, finite thickness fringes corresponding to the total thickness of the superlattice are observable, pointing out that the surface and the interfaces of the superlattice are relatively smooth. The FWHM of the zero-order satellite in q_x direction is 11 arcsec, a value corresponding to the resolution of the diffractometer. It is evident that sample No. 2 is of nearly perfect structural quality.

The ω-2θ scan of sample No. 4, which has the longest

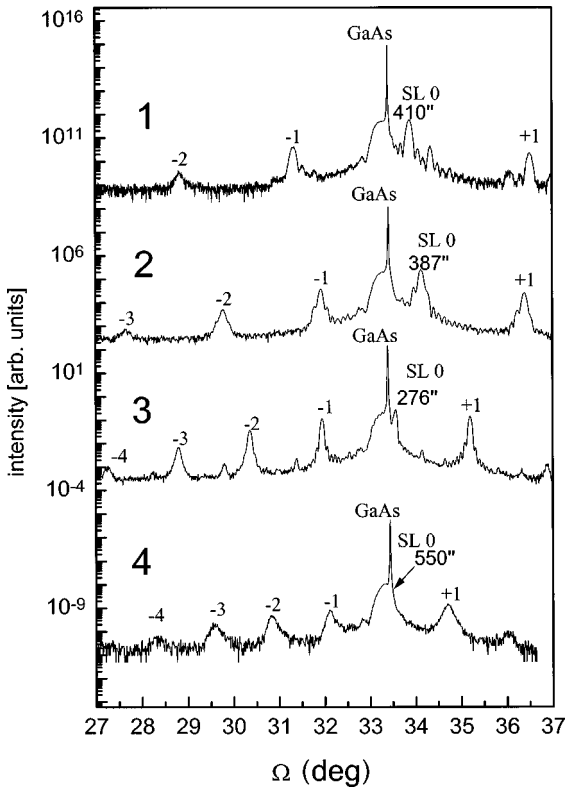

FIG. 1. ω-2θ scans of sample Nos. 1–4, measured around the 004 reflection of the GaAs substrate with HRXRD.

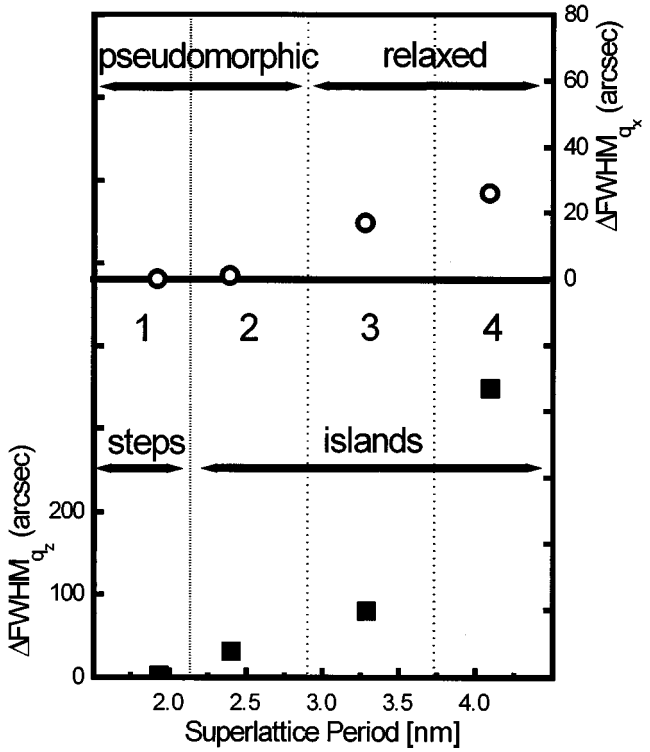

FIG. 2. Deviation from the full width at half maximum of an ideal crystal in the q_z direction (solid squares) and the q_x direction (open circles) as functions of the superlattice period.

superlattice period of the series, looks significantly different. Compared to the other samples, the satellite peaks are also of lower intensity. In addition, the superlattice satellites of sample No. 4 are broadened in the q_z direction, indicating a variation in the average vertical lattice constant. The FWHM of the zero-order satellite in the q_x direction is 36 arcsec, a value which is also significantly increased compared to the one of sample No. 2, showing that the structural quality of sample No. 4 is diminished by the formation of misfit dislocations.

All measured ω-2θ curves were simulated using the recursion relation derived from the Takagi-Taupin differential equations according to the dynamical theory of x-ray diffraction.[7,8] Since sample Nos. 1–4 have different total thicknesses and the peaks are broadened in the q_z direction due to the finite sample thickness, a variation of the lattice constant is observed as a broadening of the peaks with respect to the peak width of an ideally perfect sample (the so-called intrinsic peak width). This difference $\Delta\mathrm{FWHM}_z$ between the measured and simulated ω-2θ widths of the zero-order satellite was calculated, and taken as a suitable quantity to describe the variation of the lattice constant. In analogy, the difference $\Delta\mathrm{FWHM}_x$ between the measured FWHM in the q_x direction and the resolution of the diffractometer (which is 10 arcsec) is a measure for the mosaicity of the sample which is a consequence of the formation of misfit dislocations. The obtained values of $\Delta\mathrm{FWHM}_z$ and $\Delta\mathrm{FWHM}_x$ of the zero-order satellite of all four samples are listed in Table I.

To illustrate the results, in Fig. 2 $\Delta\mathrm{FWHM}_z$ and $\Delta\mathrm{FWHM}_x$ are plotted as functions of the superlattice period. $\Delta\mathrm{FWHM}_x$, which is a measure for the tilt in the lattice plane at a given lattice constant, also increases significantly with the superlattice period: while for sample Nos. 1 and 2 this value is zero, it is increased to 17 and 26 arcsec for sample Nos. 3 and 4, respectively. This means that the critical superlattice period determining the onset of relaxation is between 23.9 (sample No. 2) and 32.8 Å (sample No. 3).

In contrast, the $\Delta\mathrm{FWHM}_z$ is zero only for sample No. 1, while for the other three samples there exists a measurable spread in the average lattice constant. The onset of this variation in the lattice constant thus starts already *before* the onset of relaxation for superlattice periods between 19.2 (sample No. 1) and 23.9 Å (sample No. 2). The most probable interpretation for this behavior is elastic relaxation by island formation, a phenomenon that has also been observed for other strongly strained systems like InAs on GaAs, and is driven by the fact that the lattice cells at the border of the islands can expand elastically, a situation which is energetically favorable. Such an elastic relaxation typically leads to a two-dimensional wetting layer, and islands on top of it which differ in lattice constant. One would thus expect a measurable spread in the vertical lattice constant, as observed experimentally. From the experiment, one cannot distinguish whether the ZnTe or $ZnS_{0.8}Te_{0.2}$ layers form the islands. However, it is reasonable to assume that the island formation occurs in the ZnTe, which is extremely strained and thus can gain much more energy by the island formation.

In contrast to the measurements described above, in a reflectometry arrangement one probes the reciprocal space close to its origin and far away from Bragg reflections of the basic crystal lattice (in case of a superlattice, the *superlattice* Bragg peaks can, however, be much closer to the origin, and one or more superlattice Bragg peaks typically appear within the range of a reflectometry measurement). As a consequence, the method is nearly insensitive to the crystalline quality of the layers, but very sensitive to the quality of the interfaces, and thus gives information complementary to the Bragg diffraction.

Three types of information can be gained from high-resolution reflectometry: First, a scan along q_z (an ω-2θ scan) contains information on the roughness of interfaces in the vertical direction. Second, diffuse scattering in the q_x direction (obtained by an ω scan) can be evaluated to obtain lateral correlation lengths of the roughness. As in conventional Bragg diffraction, ω-2θ and ω-scans can, third, be combined to reciprocal space maps. The relative form of coherently reflected and diffusely scattered intensity gives a picture of the roughness inheritance from one layer to the next.

As a typical example, two reciprocal space maps of sample No. 3, one with the x ray parallel to the [110] direction of the substrate, and one with the x-ray perpendicular to it, are drawn in Fig. 3. The intensity of the coherent scattering is observed on a line in the ω-2θ direction along $\omega=0$. It is evident that the intensity of the diffuse scattering, which is observed at ω values away from zero, already replicates the oscillations of the Bragg reflections. This is typical of samples where the interface roughness in the vertical direction is more strongly correlated from interface to interface (so called inherited roughness), whereas uncorrelated inter-

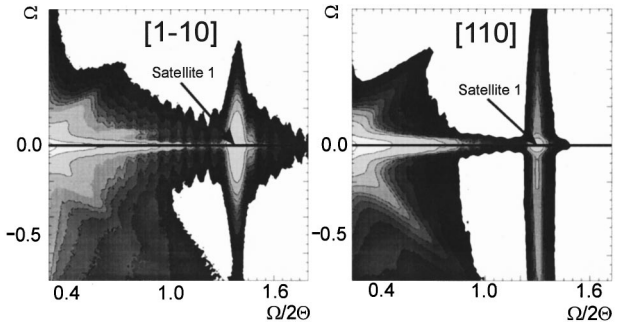

FIG. 3. Reciprocal space maps of sample No. 3, measured with an x-ray in the [1–10] and [110] directions (reflectometry).

faces would give a smooth intensity distribution of the diffuse scattering.

ω-2θ reflectometry scans correspond to a horizontal cut through the reciprocal space map at $\omega=0$. Such scans are compared in Fig. 4 for the four samples. The decay of the reflectivity curves increases with the sample number, implying that the surfaces become rougher as the superlattice periods are longer.

A quantitative evaluation of the surface and interface roughnesses can be obtained by a simulation of these curves based on the well-known Parratt's recursion relation[9]

$$R_j=\frac{r_{j,j+1}+R_{j+1}\exp(2iq_{j+1}d_{j+1})}{1+r_{j,j+1}R_{j+1}\exp(2iq_{j+1}d_{j+1})},$$

where d_j is the thickness of the jth layer, and q_j is the normal component of the wave vector inside the jth layer. The effect of the interfacial roughness is incorporated into the Fresnel reflectance[10] by

$$r_{j,j+1}=\frac{q_{j+1}-q_j}{q_{j+1}+q_j}\exp(-2q_jq_{j+1}\sigma^2),$$

where σ_j is the root-mean square of the jth interface.

Best fits based on this formalism are also shown in Fig. 4. However, it has to be stated that these fits are not unambiguous in the sense that they are not very sensitive to the difference in the roughness on top of the ZnTe and $ZnS_{0.8}Te_{0.2}$ layers. Based on the results of the high-resolution Bragg diffraction, which indicate that the ZnTe starts to form islands after a certain thickness, we used two different roughness parameters to simulate the ZnTe and $ZnS_{0.8}Te_{0.2}$ interfaces. The larger value was assumed to describe the roughness of the ZnTe layer (although good fits could also be obtained with an inverse assumption). The three resulting roughness parameters, describing the roughness of ZnTe, $ZnS_{0.8}Te_{0.2}$ and the the surface, are listed in Table II. All three roughness

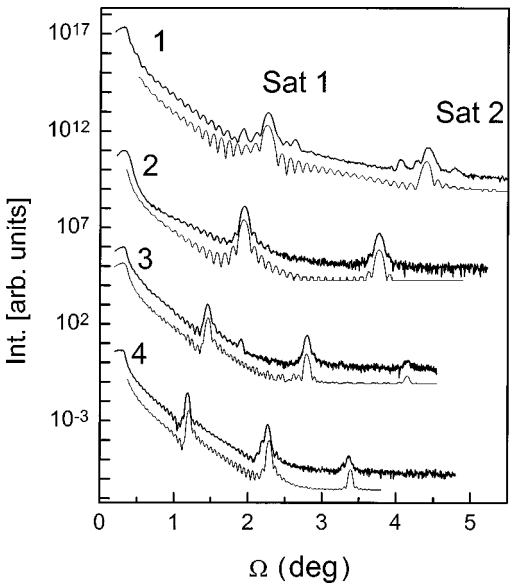

FIG. 4. ω-2θ reflectometry scans of sample Nos. 1–4 (thick line) together with fits (thin line).

parameters increase with increasing superlattice period. It also turns out that the surface is about 1 Å rougher than the interfaces. This may be due to oxidation of the surface.

The question of how the rough interfaces look like can be partly answered by ω scans through the superlattice Bragg peaks (so-called transverse scans). Such transverse scans in the q_x direction around the first-order Bragg peak were carried out in two perpendicular (110) azimuths. Figure 5 shows examples of such scans for sample Nos. 1 and 3 together with simulations based on the following formalism: The cross section for the diffuse scattering is given by[11]

$$I_{\mathrm{diff}}(q)=A\frac{|T_1T_2|^2}{|q_z|^2}\sum_{j,k}\delta_j\delta_k^*e^{-0.5q_z^2(\sigma_j^2+\sigma_k^2)}e^{-iq_z(z_j-z_k)}\times\int dr(e^{q_z^2c_{jk}(r)}-1)e^{-i(q_zx+q_yy)},$$

where $T_{1,2}$ are the transmittivities at the surface, q_z is the refraction-corrected vertical moment transfer, δ_j is the contrast in the scattering density, and A is a constant. The cross-correlation function $Cjk=\langle\Delta z_j(0,0)\Delta z_k(x,y)\rangle$ represents the average of the height-height correlations between the jth interface of height Δz_j and the kth interface of height Δz_k. This cross-correlation function can be written as[12,13]

$$C_{jk}=\sigma_j\sigma_ke^{-(z_j-z_k)/\xi_\perp}e^{-(r/\xi_\parallel)^{2h}}\cos(2\pi r/\lambda),$$

TABLE II. Roughness obtained from reflectometry and ATM.

Sample No.	$ZnTe_{Ref.}$ (Å)	$Zn(S,Te)_{Ref.}$ (Å)	$Surface_{Ref.}$ (Å)	$Surface_{AFM,\ rms}$ AM (Å)	$Surface_{AFM,\ rms}$ PM (Å)
1	3.2±0.5	2.8±0.5	4.4±0.5	6.9±2	4.1±2
2	4.0±0.5	3.2±0.5	4.7±0.5	7.1±2	3.9±2
3	4.5±0.5	3.9±0.5	5.7±0.5	7.2±2	4.2±2
4	5.6±0.5	4.5±0.5	6.2±0.5	5.4±2	4.3±2

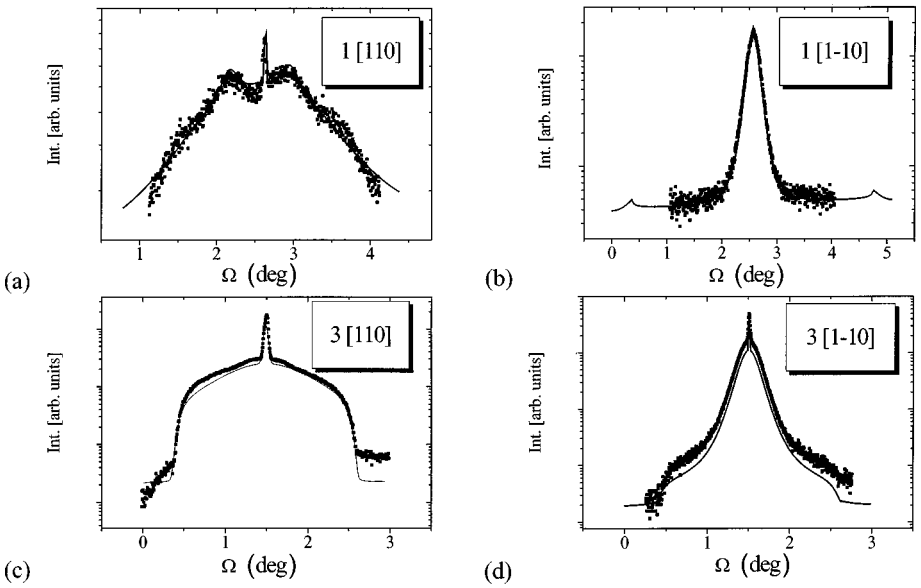

FIG. 5. ω reflectometry scans around the zero-order superlattice Bragg peak of sample No. 1 [(a) and (b)] and sample No. 3 [(c) and (d)] with an x ray parallel to the [110] direction [(a) and (c)] and to the [1−10] direction [(b) and (d)].

where $\xi_{\parallel}$ and $\xi_{\perp}$ are the mean parallel and vertical correlation lengths respectively, and h is the roughness exponent. The cosine function is introduced to account for the wavelength selection of the terraces.[14]

The scans in the two directions are very different, showing that the interface morphology is strongly anisotropic. This anisotropy can be best understood from the scans of sample No. 1, where one observes two side maximums in [110] azimuth [Fig. 5(a)]. The occurrence of such pronounced side maxima implies a wavelength selection of the roughened interfaces that can only occur if the roughness is very regular. This is typically the case for an arrangement of steps on a slightly miscut substrate. The minimum miscut angle can be directly obtained from the asymmetry of the side maxima with respect to the coherently scattered central peak; it is on the order of 0.3°. The fit in Fig. 5(a) is based on the assumption of a mean terrace width of 230 nm. Together with the miscut angle this value can be used to calculate the mean step height, which is 1.1 nm or about 3 ML. This is a strong indication that at each terrace edge several monolayer steps occur within a short distance, a well-known behavior that is called step bunching.

The peak in the [1−10] azimuth [Fig. 5(b)] is much sharper, and can be simulated with a lateral correlation length of 610 nm. The fact that side maxima do not occur in this case shows that the step distance is irregular in this direction. This is the behavior one would expect for a measurement along slightly curved terraces. The overall picture of sample 1 is thus very clear: It consists of slightly curved terraces that are limited by bunched steps in the direction transverse to the terraces.

It is interesting to observe the change of these terraces for increasing periods. The scans for sample Nos. 2–4 look qualitatively similar, so that only sample No. 3 is included Fig. 5: in the [110] direction [Fig. 5(c)], no side maxima is visible, but a broadened diffuse intensity is. From the fits one can extract that the correlation length transverse to the terraces does not change significantly, meaning that the number of terraces remains constant but their width is no longer regular. Along the terrace direction the diffuse scattered intensity has a similar shape, but is always more narrow, corresponding to larger correlation lengths. The samples are thus still anisotropic, although the anisotropy decreases with increasing period, i.e., the mean terrace length decreases.

A reasonable explanation for this behavior is the assumption that the step edges begin to become more and more curved as the period becomes larger and the strain is increased (so-called step wandering). Such a curving is energetically favorable, since it increases the fraction of lattice cells at edges, and thus allows for a certain amount of elastic relaxation. Eventually, a step curved inward and one curved outward may touch each other, forming an island that limits the terrace length. This tendency increases with increasing strain, so that the mean terrace length decreases with increasing superlattice period.

So far all conclusions have been obtained from reciprocal space, and represent an average information over a large sample area. In order to test the validity of these conclusions, it is interesting to compare the obtained picture to the results of real-space imaging techniques. AFM gives a possibility to gain information on lateral correlations and anisotropy of the surface, whereas TEM gives informations on the roughness of individual interfaces and roughness inheritance between interfaces.

As an example for the evolution of the surface with increasing period, AFM measurements of the surface of sample Nos. 1 and 3 are shown in a three-dimensional plot in Fig. 6. The image of sample No. 1 shows pronounced terraces with very regular width. The average terrace width is 200 nm, a typical step length is about 3000 nm, and the average step height is about 1 nm. With the exception of the step length, these results are in excellent agreement to the picture of regular terraces with bunched steps obtained from the x-ray reflectivity measurements. The larger terrace width from the AFM measurement (3000 nm compared to 610 nm from x-ray reflectivity) is most probably a consequence of the fact that the size of the AFM picture ($5\times5\ \mu m^2$) is too small to obtain reasonable statistics for the evaluation of average length scales.

The surface morphology of the relaxed sample No. 3 is modified, compared to sample No. 1. On the one hand, the sample still shows the typical anisotropic picture of a terrace

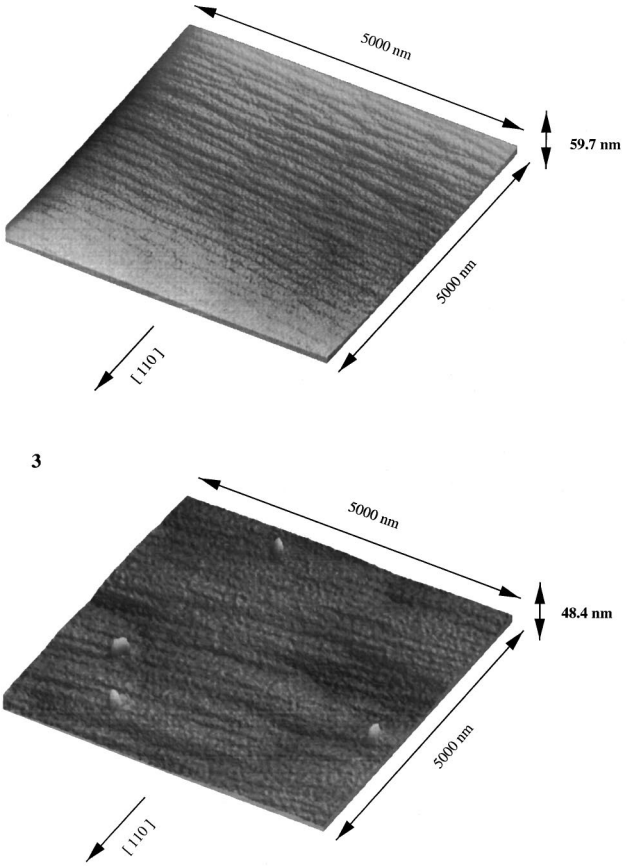

FIG. 6. Atomic force microscopy measurement of the surface of sample Nos. 1 and 3. The [110] direction is indicated.

surface, with a mean terrace width which has not changed significantly. On the other hand, the terraces have changed their size and form: They end or are eventually bent when they are close to a broader terrace. As a consequence, the anisotropy is much smaller than for sample No. 1. With the exception of the absolute values of the lateral correlation lengths (which are again larger for the AFM measurement than for the reflectivity experiment), the picture is again in good agreement to the model of terraced interfaces with wandering steps developed from the reflectivity data.

The anisotropy of the surface morphology is also revealed if one takes the rms roughness values evaluated from line scans along the [110] miscut (AM) and perpendicular to the [110]-miscut-direction (PM) into account. The corresponding values are listed in Table II. It turns out that for the sample Nos. 1, 2, and 3 the rms roughness in the AM direction is always higher than that in the PM direction (approximately 7 and 4 Å, respectively). The roughness measured within one step terrace is lower than the roughness determined perpendicular to the step edge.

Figures 7(a) and 7(b) show cross-sectional TEM images along the ⟨110⟩ projection of samples Nos. 2 and 4. The TEM image of sample No. 2 shows the GaAs buffer, followed by the 20-nm-thick ZnSe layer. On top of the ZnSe layer, the ZnTe-$ZnS_{0.8}Te_{0.2}$ superlattice structure is visible. Each superlattice period consists of a thin ZnTe layer which is darker, and a $ZnS_{0.8}Te_{0.2}$ layer which is approximately two times thicker and appears bright in the TEM image. No stacking faults and dislocations are visible in the image of

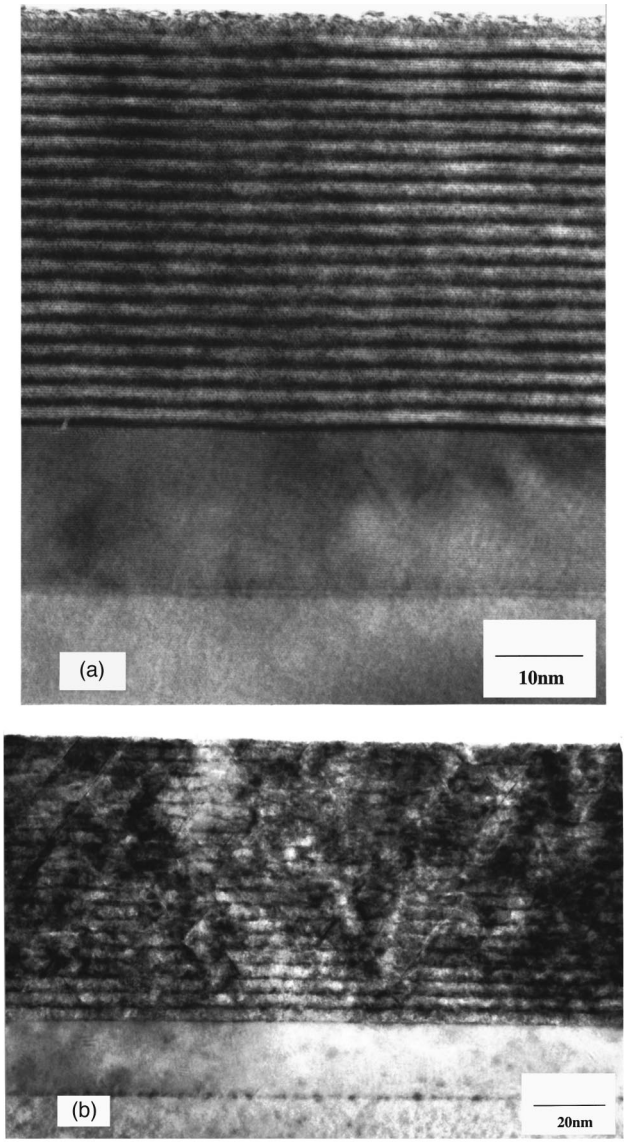

FIG. 7. Cross-sectional TEM images along the ⟨110⟩ projection of sample Nos. 2 and 4.

sample No. 2. This result agrees very well with our HRXRD measurement, because, from the FWHM of the zero-order satellite in the q_x direction of 12 arcsec, we expect that sample No. 2 is still fully pseudomorphic.

The image of sample No. 2 also allows us to compare the roughness of the ZnTe layer qualitatively with the roughness of the $ZnS_{0.8}Te_{0.2}$ layer. It is evident that ZnTe roughens the growth front, while $ZnS_{0.8}Te_{0.2}$ smooths it. Despite the smoothing effects of $ZnS_{0.8}Te_{0.2}$, the roughness of one ZnTe layer is inherited by the following ZnTe layer. These two facts are in excellent agreement with the Bragg diffraction results, which suggest island formation of the ZnTe, and the reflectivity results that show a roughness inheritance.

The cross-section TEM of the relaxed sample No. 4 looks different. The GaAs buffer and the following 20-nm ZnSe layer are similar to sample No. 2, but the perfect line pattern of a superlattice structure is disturbed. Though during the growth of the GaAs buffer and the following ZnSe layer no dislocations are visible, many dislocations are created during the superlattice growth. A detailed analysis of the TEM pic-

ture shows that these dislocations always start at a $ZnS_{0.8}Te_{0.2}$/ZnTe interface, an observation that can be understood from the fact that the critical thickness for ZnTe is much lower than that for $ZnS_{0.8}Te_{0.2}$, so that relaxation occurs first in the ZnTe.

SUMMARY

In conclusion, we have applied high-resolution x-ray techniques to investigate crystallinity and interface properties of $ZnS_{0.8}Te_{0.2}$/ZnTe strain-balanced superlattices as a function of their period. To gain a conclusive picture, it is necessary to probe the reciprocal space in different regions: Measurements around the (004) Bragg peak alow conclusions on island formation and relaxation: For a superlattice period below 2 nm the layers and interfaces are nearly perfect. At periods above 2 nm there is a spread in the average lattice constant, indicating the formation of ZnTe islands. Finally, at periods above 2.4 nm the critical thickness of the ZnTe layers is exceeded, and dislocations are observed as a spread in the lattice plane orientation. Reflectometry scans, that probe a region close to the origin of reciprocal space, give complementary information and help to quantify the interface roughness: The nearly perfect sample with the lowest period exhibits a pronounced structure of very regular terraces with bunched steps, so that the interfaces are strongly anisotropic. The roughness in the vertical direction is very low, and is inherited from layer to layer. With increasing period, one observes an increase of the vertical roughness due to island formation and a decrease of the anisotropy due to step wandering. Direct imaging methods like AFM and TEM essentially confirm these results, but do not give much additional information. We think that our work underlines the usefulness of x-ray scattering for the analysis of interfaces.

ACKNOWLEDGMENTS

We thank Dipl. Phys. We. Send (University of Karlsruhe) for the TEM analysis. This work was supported by BMBF, SFB 410, and FOROPTPO.

[1] M. A. Haase, J. Qui, J. M. DePuydt, and H. Cheng, Appl. Phys. Lett. **59**, 1272 (1991).
[2] M. Ehinger, C. Koch, M. Korn, D. Albert, N. Nürnberger, V. Hock, W. Faschinger, and G. Landwehr, Appl. Phys. Lett. **73**, 24 (1998).
[3] I. K. Sou, K. S. Wong, Z. Y. Yang, H. Wang, and G. K. L. Wong, Appl. Phys. Lett. **66**, 1915 (1995).
[4] W. Faschinger, M. Ehinger, T. Schallenberg, and M. Korn (to be published).
[5] M. Korn, T. Gerhard, H. R. Ress, D. Albert, A. Gerhard, C. Schumacher, and W. Faschinger, J. Cryst. Growth **184/185**, 62 (1998).
[6] S. K. Sinha, E. B. Sorita, S. Garoff, and H. B. Stanley, Phys. Rev. B **38**, 2297 (1988).
[7] S. Takagi, Acta Crystallogr. **15**, 1311 (1962).
[8] D. Taupin, Bull. Soc. Fr. Mineral. Cristallogr. **87**, 469 (1964).
[9] L. G. Parratt, Phys. Rev. **95**, 359 (1954).
[10] H. Dosch, *Critical Phenomena at Surfaces and Interfaces*, Springer Tract in Modern Physics, Vol. 126 (Springer, New York, 1992).
[11] V. Holy and T. Baumbach, Phys. Rev. B **49**, 10 668 (1994).
[12] Z. H. Ming, A. Korl, Y. L. Soo, Y. H. Kao, J. S. Park, and K. L. Wang, Phys. Rev. B **47**, 16 373 (1993).
[13] T. Gu, A. I. Goldman, and M. Mao, Phys. Rev. B **56**, 6474 (1997).
[14] Y.-P. Yao, H.-N. Yang, G.-C. Wang, and T.-M. Lu, Phys. Rev. B **57**, 1922 (1998).